




Generating overlap between compass states and squeezed, displaced, or Fock states

Arman ^{1,*} and Prasanta K. Panigrahi ^{1,2,†}

¹*Department of Physical Sciences, Indian Institute of Science Education and Research Kolkata, Mohanpur-741246, West Bengal, India*

²*Centre for Quantum Science and Technology (CQST), Siksha 'O' Anusandhan Deemed to be University, Khandagiri Square, Bhubaneswar-751030, Odisha, India*

 (Received 26 March 2023; revised 9 October 2023; accepted 20 February 2024; published 25 March 2024)

We investigate a broad class of nonclassical states, composed of superposed squeezed and displaced number states. The phase-space structure is analyzed, keeping in mind the Heisenberg limited sensitivity in parameter estimation. Appropriate squeezing and displacement parameters are identified, wherein the state fidelity in comparison to the metrologically sensitive compass state is more than 99%. Also, the equal variance in small shift measurements, for the proposed and compass state, shows identical behavior of the average photon number. In metrological application, the number variance of the compass state, which is small for low coherent amplitude, suggests its potential to estimate damping parameters. Finally, we present the theoretical models corresponding to their preparation.

DOI: [10.1103/PhysRevA.109.033724](https://doi.org/10.1103/PhysRevA.109.033724)

I. INTRODUCTION

Coherent states are minimum uncertainty states with the Poissonian statistics in the Fock space, describing their classical nature. The superposition of four different coherent states [1] is known as the compass or kitten state (KS). See Ref. [2] for the choice of label “KS.” The compass state (KS) possesses sub-Planck scale structures in the phase space with oscillatory distribution as a function of small quadrature phase-space shift ($\delta x, \delta p$). The interferometric phase-space structure makes the KS sensitive to quadrature fluctuation, therefore allowing the detection of weak external forces [3,4] as well as quadrature phase fluctuation [5,6]. This behavior of oscillation can be realized in the experiment by measuring the inversion of a two-level system (TLS) entangled with the cavity system maintained in the compass state as a probe [6–8]. In this process, the atom and field system interact in a way such that the inversion of TLS becomes proportional to the Wigner function of the system. This whole process allows us to measure the sensitivity of the probe system in terms of small phase-space perturbation [8]. Due to the high sensitivity of KS against loss of the interferometric structure or non-classicality in the presence of damping to the environment, it presents great potential as a probe in estimating the damping constant of the system.

The need for the generation of highly nonclassical states [9–11] for advancement in fault-tolerant continuous-variable quantum computation, information processing, and communication has become pertinent in the optical as well as microwave [12] platforms. The cat, compass, and higher order of n superposition coherent states (quantum hypercube state [13]) have found their uses as cat codes in quantum error correction (QEC) due to the property of returning to

the same state after two, four, and n excitation loss, respectively [14–16]. Encoding logical qubits in higher-dimensional Hilbert space of bosonic systems, suffering a few natural errors, has allowed the preparation of QEC systems, preserving them over a longer period and achieving fault-tolerant systems. The large amplitude of these bosonic states increases the success of correcting errors in the logical qubit. There have been many proposals [17–19] and experimental [20] generation of low-amplitude cat states in microwave [21] as well as optical [22] platforms; however, with very few proposals [23,24], it remains a challenge for the preparation of high-fidelity large-amplitude cat, KS, as well as n -coherent states. This motivates us to find new methods for producing a state with an achievable and possibly optical setup.

In this paper, we study the phase-space structures (Sec. III) for two states proposed in Sec. II, investigating the probability number distribution (PND) for both squeezing and displacement parameters. The squeezing is not limited to its uses in a single mode, as recently shown for a two-mode squeezing superposition [25] with metrological aspects and ion trap implementation. Additionally, we analyze the fidelity between the proposed states and the compass state in Sec. IV, and propose a theoretical model for their preparations in Sec. VI. Finally, Sec. VII contains a conclusion with a summary.

II. SUPERPOSITION OF SQUEEZED AND DISPLACED NUMBER STATES

The main aim of this paper is finding the form of states in such a way that there exists a large overlap of KS with the states comprised of squeezing, displacement, and Fock number parameters. We know that the photon-subtracted squeezed state ($\hat{a}S[r]|0\rangle$) is equivalent to the squeezed single-photon state ($S[r]|1\rangle$), and describes two Gaussian lobes with negative center in the phase space causing large overlap with the odd cat state [17]. Using this analogy, we have two approaches to obtain KS with possibly large overlap: (i) application of squeezing on two different displacements for the Fock state or

*a19rs004@iiserkol.ac.in

†Corresponding author: pprasanta@iiserkol.ac.in

(ii) two opposite phase-space oriented squeezings of the Fock state.

We express the mathematical form of the two proposed states in the x -projected space before assessing the qualitative characteristics, such as probability number distribution and phase-space distribution, as well as quantitative metrics, such as fidelity. The first state is a combination of squeeze and displacement operators acting on the number state. The expression for the squeezed superposed displaced number state (SSDNS) with displacement (α) and squeezing (r) parameters is as follows:

$$|\psi_1\rangle = N_1 S[r](D[\alpha] + D[-\alpha])|n\rangle,$$

where N_1 and $D[\alpha]$ are the normalization and displacement operator with α being real, respectively. The other state involves a superposition of two squeezed number states with opposite signs of the squeezing parameter r . The superposed squeezed number state (SSNS) is expressed as follows:

$$|\psi_2\rangle = N_2(S[r] + S[-r])|n\rangle.$$

In this case, N_2 stands for the normalization factor and $S[r]$ is the squeezing operator denoted by the expression $e^{r\frac{a^2 - a^{\dagger 2}}{2}}$, where r is real. Knowing the form of normalized oscillator state $|n\rangle$ in terms of the Hermite polynomial $H_n(x)$ of the order of n , in x -projection $\phi_n(x) = \langle x|n\rangle$, the squeezed displaced Fock state is written as

$$\begin{aligned} \phi_n(e^r x - \alpha) &= \langle x|S[r]D[\alpha]|n\rangle \\ &= \frac{\sqrt{e^r} e^{-\frac{1}{2}(-\sqrt{2}\alpha + e^r x)^2} H_n(e^r x - \alpha\sqrt{2})}{\sqrt{2^n n! \sqrt{\pi}}}, \end{aligned}$$

leading to the representation of both states in x space as $\psi_1(x) = \langle x|\psi_1\rangle = N_1[\phi_n(e^r x - \alpha) + \phi_n(e^r x + \alpha)]$ and $\psi_2(x) = \langle x|\psi_2\rangle = N_2[\phi_n(e^r x) + \phi_n(e^{-r} x)]$. Using the x -space projections, we perform detailed calculations for number distribution, Wigner function, and small shift variances (see Appendix B).

For investigating the statistical properties of both states, we plot the PND (see Fig. 1) with the obtained Fock-space representation as

$$|\psi_1\rangle = \sum_{m=0}^{\infty} c_m |m\rangle \quad \text{and} \quad |\psi_2\rangle = \sum_{m=0}^{\infty} b_m |m\rangle,$$

where c_m and b_m are probability amplitudes. In Fig. 1, the PND is denoted as $P(m)$, which is $|c_m|^2$ for ψ_1 and $|b_m|^2$ for ψ_2 .

Furthermore, to explore and obtain the large similarity via qualitative and quantitative properties for the pairs of proposed and KS states, we look for the relevant form of KSs corresponding to the ' n ' parameter-dependent ψ_1 and ψ_2 . The l orthogonal states can be constructed for l superposed coherent states with an appropriate weight factor [14]. In Fock space, four orthogonal KSs with β amplitude and label

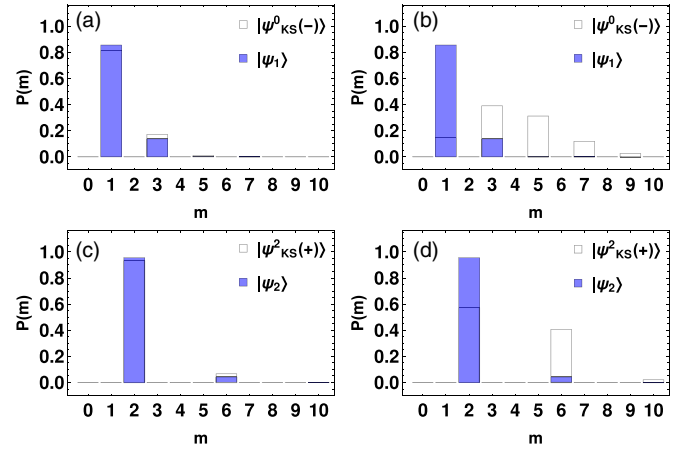


FIG. 1. Comparative PND analysis for SSDNS vs KS states. (a) Strong overlap in PND plot between SSDNS ψ_1 and $\psi_{KS}^0(-)$ with parameters $(r, \alpha, n, \beta) = [0.15, 0.61, 1, 0.75(1 + i)]$, suggesting potential squeezing and displacement strength for proximity to the KS state. (b) Reduced overlap with $\beta = 2$, while other parameters remain constant. (c) PND comparison of SSNS ψ_2 and KS $\psi_{KS}^2(+)$ with parameters $(r, n) = (0.3, 2)$ and $\beta = 1.5$ reveals substantial similarity. (d) Noticeably decreased overlap as β for the KS state becomes 2.

$l \in \{0, 1, 2, 3\}$ are written as

$$\begin{aligned} |\psi_{KS}^l(\pm)\rangle &= |\beta\rangle \pm (-1)^{-l} |-\beta\rangle + (i)^{-l} |i\beta\rangle \pm (-i)^{-l} |-i\beta\rangle \\ &= \left(\sum_{p=0}^{\infty} |f_p^\pm|^2 \right)^{-\frac{1}{2}} \sum_{m=0}^{\infty} f_m^\pm |m\rangle, \end{aligned}$$

where

$$f_m^+ = \frac{\beta^{4n+l} \delta_{m,4n+l}}{\sqrt{(4n+l)!}}, \quad f_m^- = \frac{[1 + (-1)^n i] \beta^{2n+l+1} \delta_{m,2n+l+1}}{\sqrt{(2n+l+1)!}}.$$

In the above expression, l ranges from 0 to 3 and 0 to 1 for $|\psi_{KS}^l(+)\rangle$ and $|\psi_{KS}^l(-)\rangle$, possessing four and two orthogonal states, respectively. It becomes clear for the choice of two different KSs when their PNDs are compared with our proposed states. PNDs for both states against Fock-state number " m " are seen in Fig. 1. Both compass $|\psi_{KS}^l(-)\rangle$ and SSDNS $|\psi_1\rangle$ possess odd distribution [see Figs. 1(a) and 1(b)] for $n = 1$ and $l = 0$, which changes to even parity for n even and $l = 1$. In Fig. 1(a), the PND overlap is high between $|\psi_{KS}^l(-)\rangle$ and $|\psi_1\rangle$, while in Fig. 1(b), it reduces with a change in β . Both states show their distribution similar to the cat state, where nonzero adjacent states are at a step of 2 along Fock state $|m\rangle$ for either even or odd parity. Figures 1(c) and 1(d) describe, respectively, the large and small overlap of the PNDs between compass $|\psi_{KS}^l(+)\rangle$ and SSNS $|\psi_2\rangle$ for $n = 2$ and $l = 2$. They possess even distribution at a step of 4 along Fock state $|m\rangle$. Even and odd parity correspond to even and odd values of n and l for both KS and ψ_2 . Considerable overlap between the compass state and our proposed state for number distribution is obtained by tuning squeezing, displacement, and n parameters for appropriate output of the coherent amplitude β . Further, analyzing the Wigner distribution allows us to view whether there exist interferometric structures with sub-Planck scales and regular oscillations.

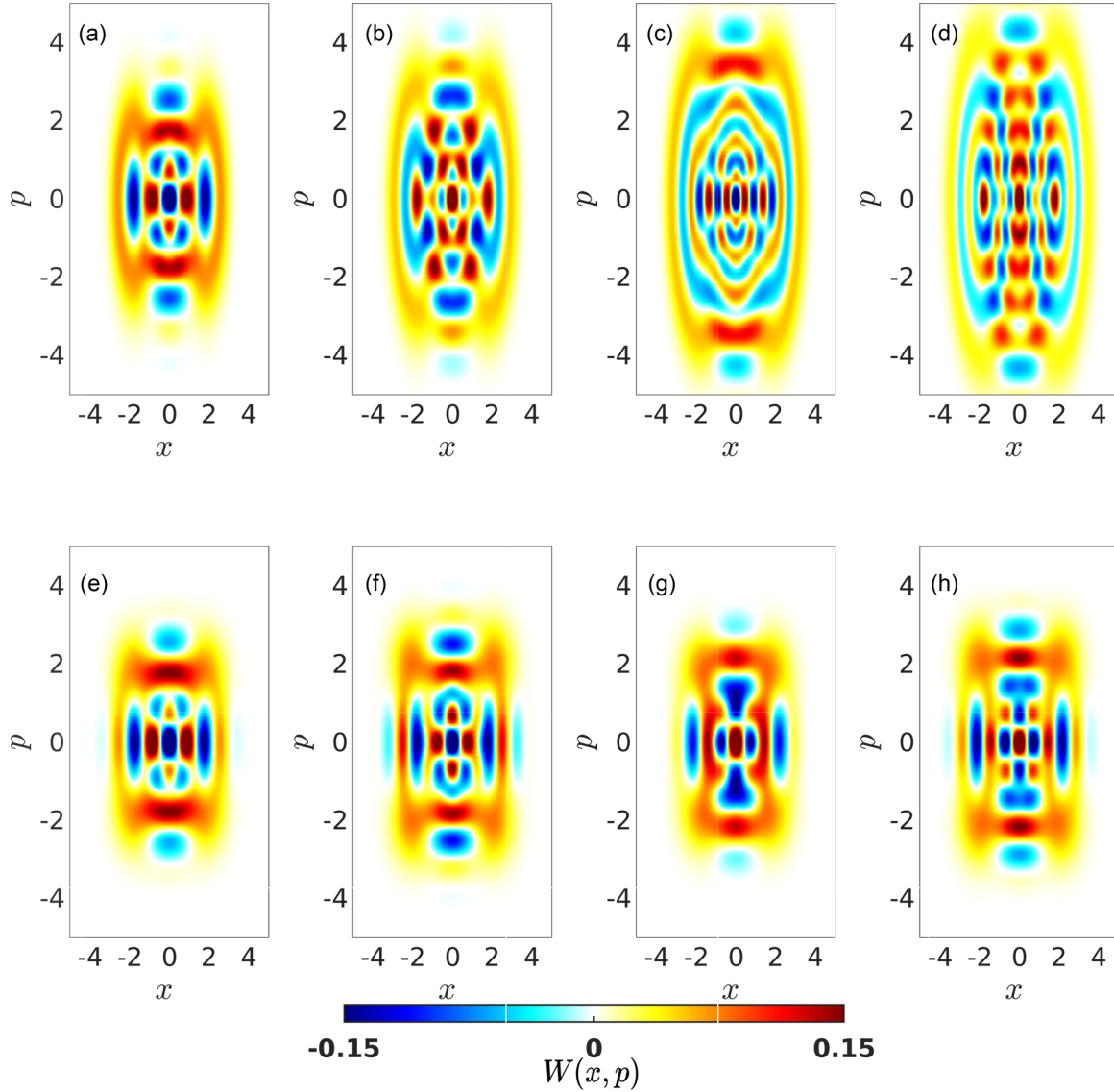


FIG. 2. The interference appears in the Wigner function of SSDNS for squeezing $r = 0.45$ and displacement $\alpha = 2$ for different Fock number: (a) $n = 1$, (b) $n = 2$, (c) $n = 3$, (d) $n = 4$. The phase-space distribution for (a)–(d) is compared with two different KS, $\psi_{\text{KS}}^0(-)$ and $\psi_{\text{KS}}^1(-)$. We present the plots of KS $\psi_{\text{KS}}^0(-)$ with parameters (e) $\beta = 1.7e^{3i\pi/4}$ and (f) $\beta = 2e^{3i\pi/4}$. Additionally, we provide the plots of KS $\psi_{\text{KS}}^1(-)$ for (g) $\beta = 1.7e^{3i\pi/4}$ and (h) $\beta = 2e^{3i\pi/4}$.

III. WIGNER FUNCTION

The Wigner function is the quasiprobability distribution in the phase space as one of the measures for nonclassicality depending upon its negative volume. The presence of positive and negative parts in this distribution signifies the displaced parity of the state. The Wigner function is derived as follows:

$$W_j(x, p) = \frac{1}{\pi} \int_{-\infty}^{\infty} dy \langle x - y | \psi_j \rangle \langle \psi_j | x + y \rangle e^{2ipy},$$

where $W_1(x, p)$ and $W_2(x, p)$ are the Wigner functions for SSDNS ψ_1 and SSNS ψ_2 corresponding to $j = 1$ and 2 , respectively.

In this section, the reason for the proposed states SSDNS and SSNS becomes evident as we compare their phase-space distributions with the corresponding KS states $\psi_{\text{KS}}^l(-)$ and $\psi_{\text{KS}}^l(+)$.

As illustrated in Figs. 2(a)–2(d), we present the phase-space distributions of SSDNS for various values of n ranging from 1 to 4. Additionally, Figs. 2(e) and 2(f) display the phase-space distributions for KS $\psi_{\text{KS}}^0(-)$, while Figs. 2(g) and 2(h) show those for KS $\psi_{\text{KS}}^1(-)$. It is worth noting that in Figs. 2(e)–2(h), the KS states exhibit central interference patterns around the origin, characterized by four Gaussian lobes at the corners of a square.

This structure can be understood as arising from the displacement of squeezed Fock states ($S[r]|n\rangle$), at two positions, namely, α and $-\alpha$, along the real quadrature, as depicted in Figs. 2(a)–2(d). Here, it is important to emphasize that $S[r]|n\rangle$ almost represents the cat state, with its amplitude increasing as n varies under suitable squeezing parameter r .

Interestingly, both Figs. 2(e) and 2(f) display a strong resemblance in their distributions to SSDNS in Fig. 2(a). Similarly, the plots in Figs. 2(g) and 2(h), as β increases,

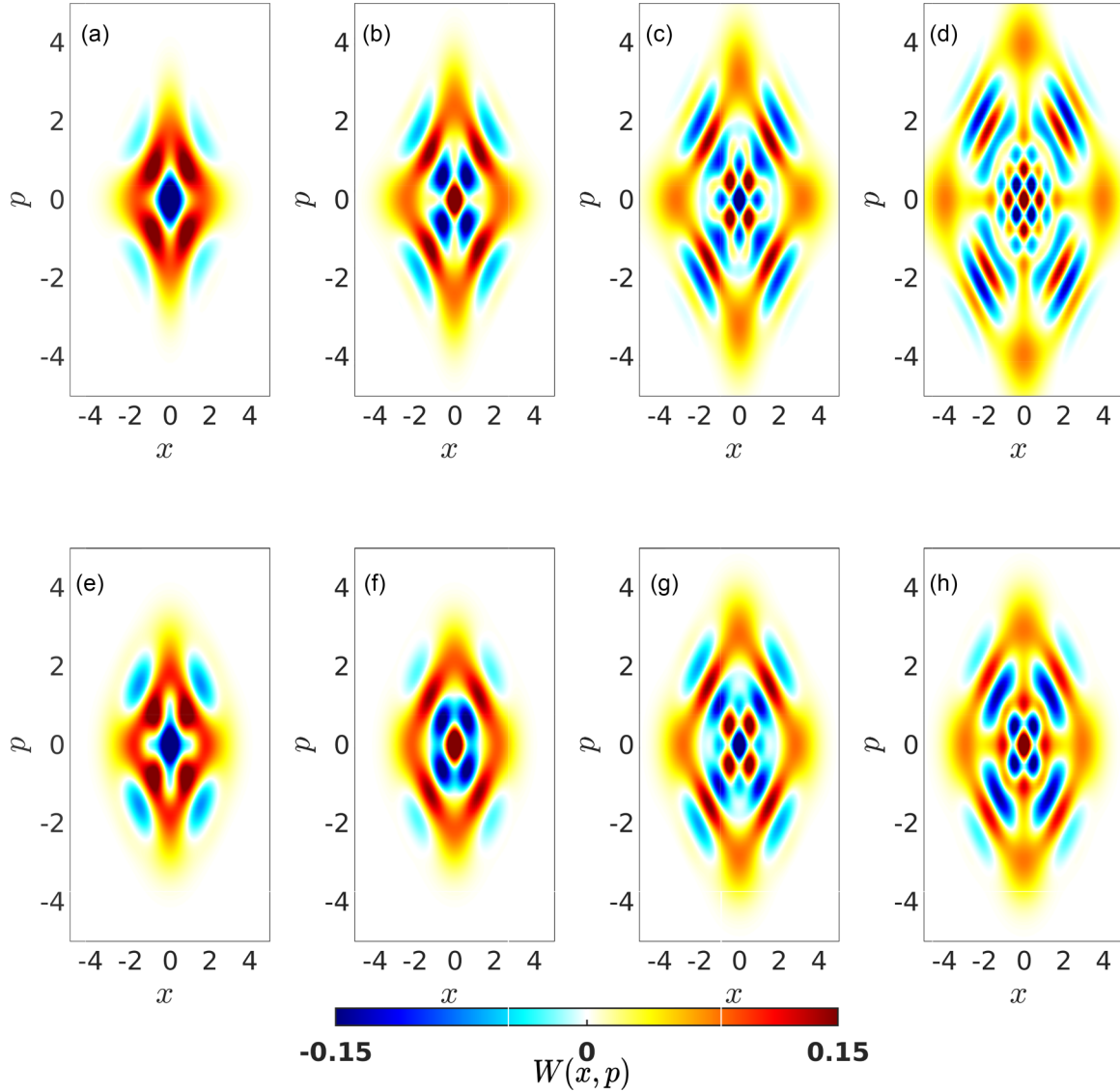


FIG. 3. The sub-Planck scale structure appears in the phase space of SSNS for squeezing $r = 0.45$ with Fock number (a) $n = 1$, (b) $n = 2$, (c) $n = 3$, (d) $n = 4$, as well as in the same distribution for different KSs: (e) $\psi_{\text{KS}}^1(+)$, (f) $\psi_{\text{KS}}^2(+)$ with $\beta = 1.5$, and (g) $\psi_{\text{KS}}^3(+)$, (h) $\psi_{\text{KS}}^4(+)$ with $\beta = 2$. Significant similarity is observed between plots of pairs: (a) and (e), (b) and (f), (c) and (g), and (d) and (h).

demonstrate analogous distribution patterns around the origin, characterized by four Gaussian lobes at the corners of a rectangle, mirroring the SSDNS in Fig. 2(b). It is noteworthy that the excess fringes observed in SSDNS for $n = 2$ [Fig. 2(b)] lead to a reduction in overlap with KS states in Figs. 2(g) and 2(h).

This analysis underlines the importance of optimizing the overlap between SSDNS and KS by adjusting the parameters r , α , and β , as elaborated in Sec. IV. Furthermore, Figs. 2(c) and 2(d) do not exhibit a substantial degree of resemblance in their distributions with either of the KSs in Figs. 2(e)–2(h). This observation highlights the diminishing overlap between KSs and SSDNS as n increases (see details of the fidelities in Sec. IV and Appendix A).

Furthermore, we elucidate the motivation for proposing the second state, which involves squeezing the number state ($S[|r|e^{i\phi}]|n\rangle = e^{|r| \frac{-i\phi\alpha^2 - e^{i\phi}\alpha^2}{2}} |n\rangle$). The direction of squeezing

applied to the number state is tuned in the phase space via the squeezing angle (ϕ). Consequently, to achieve a phase-space distribution akin to that of the KS, it necessitates the implementation of two squeezing operations of equal magnitude, with a phase difference of π in the phase space, leading to the superposition of two squeezing operators acting on the Fock state $|n\rangle$ (SSNS).

The Wigner function $W_2(x, p)$ of the SSNS distinctly manifests sub-Planck oscillatory behavior, as seen in Figs. 3(a)–3(d), corresponding to different values of n , ranging from 1 to 4. A comparison of these $W_2(x, p)$ distributions in Figs. 3(a)–3(d) is made with the distributions for KSs denoted as $\psi_{\text{KS}}^l(+)$, where l varies from 1 to 4, as illustrated in Figs. 3(e)–3(h).

For the real amplitude parameter β of the KSs, we observe a remarkable similarity in terms of interference patterns and the presence of Gaussian lobes when comparing pairs of distributions: Figs. 3(a) and 3(e), Figs. 3(b) and 3(f), Figs. 3(c)

TABLE I. Fidelities of SSDNS and SSNS vs KSs.

State $\mathcal{F}_\psi^{(l,\pm)}$	α	n	r	KS (β)	Fidelity ($\mathcal{F}_\psi^{(l,\pm)}$)
$\mathcal{F}_{\psi_2}^{(3,+)}$	0	3	0.2	1.41	0.9998
$\mathcal{F}_{\psi_2}^{(2,+)}$	0	2	0.3	1.41	0.9997
$\mathcal{F}_{\psi_2}^{(1,+)}$	0	1	0.3	1.01	0.9994
$\mathcal{F}_{\psi_2}^{(0,+)}$	0	0	0.4	0.81	0.9998
$\mathcal{F}_{\psi_1}^{(0,-)}$	0.61	1	0.15	$0.7(1+i)$	0.9995
$\mathcal{F}_{\psi_1}^{(0,-)}$	0.7	1	0.2	$0.85(1+i)$	0.9960
$\mathcal{F}_{\psi_1}^{(-1,-)}$	0.5	2	0.49	$0.9(1+i)$	0.9634

and 3(g), and Figs. 3(d) and 3(h). Increase in the fringes and phase-space area of the SSNS [Fig. 3(d)] compared to KS [Fig. 3(h)] causes reduced overlap (see details of the fidelities in Sec. IV and Appendix A).

In addition to our qualitative analysis, the subsequent section deals with a quantitative examination, specifically focusing on fidelity as a suitable measure for the closeness of our states to KS. Moreover, the fidelity as an overlap between perturbed and unperturbed states serves as a sensitivity for estimating minute shifts within the phase space. To elaborate, both overlap and variance in measurements of displacement due to small phase-space perturbations enable us to investigate a rigorous comparison of our proposed states with KS.

IV. FIDELITY AND SMALL SHIFT SENSITIVITY

To assess the degree of similarity between states ψ_1 and ψ_2 and the KS states for large amplitudes ($|\beta| > 0.5$), where small area phase-space structures are present in both field quadratures, we use a measure known as fidelity (\mathcal{F}_ψ). Fidelity quantifies the closeness or overlap between a target state and an acquired state, serving as a metric for comparing their similarity.

This fidelity measure, denoted as \mathcal{F}_ψ for the proposed state $|\psi\rangle$ and the KS state $|\psi_{\text{KS}}^l(\pm)\rangle$, is expressed in terms of squeezing and displacement parameters as follows:

$$\mathcal{F}_{\psi_1}^{(l,\pm)} = |\langle \psi_1 | \psi_{\text{KS}}^l(\pm) \rangle|^2$$

and

$$\mathcal{F}_{\psi_2}^{(l,\pm)} = |\langle \psi_2 | \psi_{\text{KS}}^l(\pm) \rangle|^2.$$

The precision measurement processes are dependent on the energy resources, for example, average of photon number $\langle n \rangle$ of the probe state. In the standard quantum limit (SQL), small displacement measurements are independent of the average of the photon number, using coherent state as a probe, while the presence of sub-Planck structures in the probe state (such as cat state and compass state of coherent amplitude β) allows measurement of the small displacement $[\delta = \sqrt{2}(\delta x + i\delta p)]$ inversely proportional to the coherent amplitude $|\beta|$ (where $|\beta| \sim \sqrt{\langle n \rangle}$ with $|\beta| > 2$ for the cat and KS states), which leads to Heisenberg limited sensitivity (HL) [3,6,8]. We know from Table I of the fidelities for both proposed states with KS that tuning to particular values of squeezing r and displacement α parameters for Fock number $n = 1$ provides overlap beyond 99%. For SSDNS with $n = 1$, we find great fidelity for different coherent amplitude β of the KS ($|\psi_{\text{KS}}^l(-)\rangle$), while

other values of n for this state do not make good candidates for the comparison with KS on the basis of overlap (\mathcal{F}_ψ). Our second state (SSNS) for every Fock number ($n = 0, 1$ and so on) shows fidelity beyond 99% with the KS ($|\psi_{\text{KS}}^l(+)\rangle$) for different coherent amplitude (β).

Further, we compare the sensitivity of small phase-space shifts for SSDNS, SSNS, and KS with the help of the overlap quantity.

Overlap (O_{v_δ}) of perturbed and unperturbed states of the system describes distinguishability of the state distribution against small shifts in phase space and quantifies sensitivity to the shifts δ as $O_{v_\delta} \rightarrow 0$ with $\delta \rightarrow \delta_0$ (first zero of O_{v_δ}). Hence, the sensitivity of state is how quickly the overlap (O_{v_δ}) changes with a small change in shift δ . The smaller the overlap

$$\begin{aligned} O_{v_\delta} &= 2\pi \int_{-\infty}^{\infty} dx dp W_\psi(x, p) W_\psi(x + \delta x, p + \delta p) \\ &= |\langle \psi | D[\delta] e^{i\theta} | \psi \rangle|^2 \sim 1 - \frac{1}{4} F_Q(\psi) |\delta|^2 + O(|\delta|^3) \end{aligned}$$

becomes for different states ψ , the higher the sensitivity against the same weak perturbations δ ($= |\delta| e^{i\theta}$) in the phase space becomes. Above expansion O_{v_δ} is applicable for small $|\delta|$ with negligible higher-order terms $O(|\delta|^3)$. The term $F_Q(\psi)$ characterizes the rate of change in O_{v_δ} . Therefore, this term itself is a measure of sensitivity, known as quantum Fisher information, [26] for probe state ψ . A larger value of $F_Q(\psi)$ corresponds to a reduced δ_0 , which in turn results in higher sensitivity. Later in this section, we find that the variance in estimating $|\delta|$ is inversely proportional to F_Q . This relation is also known from the quantum Cramer-Rao bound, where the root-mean-square error in parameter estimation is bounded below by the inverse of its Fisher information [27].

We now focus on the estimation of small displacements with a two-level system (TLS). The overlap of the system state is obtained by measurement of the TLS, interacting with the probe state ($|\psi\rangle$) of the system, either in the upper state ($|e\rangle$) or lower state ($|g\rangle$).

In the measurement strategy of small displacements, a probe state of the oscillator (field state or ion state) entangled with TLS is prepared through time unitary evolution U by initializing the system in the product state of the oscillator ($|\phi_i\rangle$) and TLS ($|e\rangle$). After the preparation, small displacement operator $D[\delta]$ as a consequence of weak forces or small perturbations external to the composite system (oscillator and TLS) is applied along with reversing the action of U thereafter. The final state ($|\psi_f\rangle$) obtained for this composite system [6] is written as

$$|\psi_f\rangle = U^{-1} D[\delta] U |\phi_i\rangle |e\rangle = \sqrt{p_e} |\Phi_1\rangle |e\rangle + \sqrt{p_g} |\Phi_2\rangle |g\rangle.$$

The U unitary operator is such that probe state $|\psi\rangle$ and the excited state probability

$$p_e = |\langle e | \langle \phi_i | \psi_f \rangle \langle \phi_i | \Phi_1 \rangle|^2 = |\langle \psi | D[\delta] | \psi \rangle|^2 = O_{v_\delta}.$$

We can take the advantage of preparing probe state $|\psi\rangle$ into either the cat state, compass state (KS), SSDNS, or SSNS. In the measurement of a two-level atom in the excited state, the obtained probability function [$p_e = p_e(\delta)$] is inverted to find small shift δ . To achieve an estimated small displacement very close to its true value, a measurement of the TLS of the composite system, in its excited or ground state, is repeated R

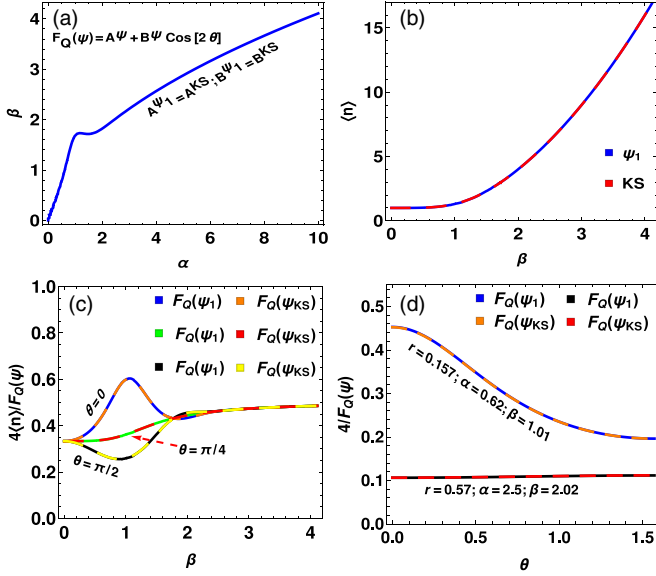


FIG. 4. Comparative variance and average photon number $\langle n \rangle$ analysis for SSDNS vs KS: (a) Blue line follows $F_Q(\psi_1) = F_Q(\psi_{KS}^0(-))$ leading to two constraints $A^{\psi_1} = A^{KS}$ and $B^{\psi_1} = B^{KS}$. This curve corresponds to equal variance for SSDNS with $n = 1$ and $\psi_{KS}^0(-)$, with β being the absolute of coherent amplitude $\beta e^{i\pi/4}$. (b) $\langle n \rangle$ and (c) product of variance and $\langle n \rangle$ become the same for constraints in (a), at each θ with respect to SSDNS and $\psi_{KS}^0(-)$. (d) Both states have the same variance changing with θ at small $\beta = 1.01$ and remain constant at $\beta = 2.02$.

times. Consider m times ($m \ll R$) the atom is found to be in its excited state. The probability of this measurement is written [6,8] as

$$\frac{R!}{m![(R-m)!]} p_e^m (1-p_e)^{R-m},$$

where this binomial can be approximated to normal distribution, when number R is very large compared to m . With prior knowledge of $0 < \delta < \delta_0 \ll 1$ and true value $s = |\delta|^2$, the normal distribution in terms of R , p_e is

$$\frac{1}{\sqrt{2\pi\Delta_s^2}} e^{-\frac{(s-\bar{s})^2}{2\Delta_s^2}},$$

where \bar{s} is the estimated value of shifts, with variance

$$\Delta_s^2 \sim \frac{4|\delta|^2}{RF_Q(\psi)}.$$

The smaller the variance, the closer the estimator (\bar{s}) to the true value (s), as seen in the above normal distribution. We calculate variances Δ_s^2 and average number $\langle a^\dagger a \rangle$ for ψ_1 , ψ_2 , and ψ_{KS} as probe states, against variation in squeezing (r), displacement (α), and Fock number (n) along with the amplitude $|\beta|$ of the KS. We approximated the variance to $4|\delta|^2/(RF_Q) < 4|\delta_0|^2/(RF_Q) < 4/(RF_Q)$, with quantum Fisher information F_Q dependent on the parameters of the probe state (ψ). We have that F_Q only produces a change in variance Δ_s^2 for different states ψ . Therefore, we plot quantity $4/F_Q$ as the variance and average photon number $\langle n \rangle$ for the compass state (ψ_{KS}), SSDNS (ψ_1), and SSNS (ψ_2) in Figs. 4 and 5 to study their energy cost in perturbation sensitivity. Here, the energy cost signifies the average amount of the energy resources occupied

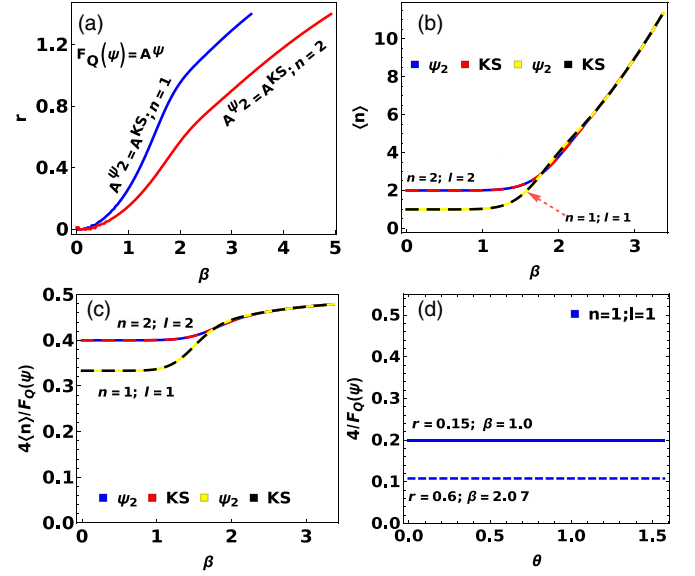


FIG. 5. Comparative variance and average photon number $\langle n \rangle$ analysis for SSNS vs KS: (a) Both curves follow $F_Q(\psi_2) = F_Q(\psi_{KS}^1(+))$, leading to a constraint $A^{\psi_2} = A^{KS}$. Blue curve corresponds to equal variance for SSNS with $n = 1$ and $\psi_{KS}^1(+)$, with β being the coherent amplitude. Similarly, the red curve describes the same variance for SSNS with $n = 2$ and $\psi_{KS}^2(+)$. The following pairs: SSNS $n = 1$ (yellow) and $\psi_{KS}^1(+)$ (black), and SSNS $n = 2$ (blue) and $\psi_{KS}^2(+)$ (red), have overlapping lines for (b) $\langle n \rangle$ and (c) the variance multiplied by $\langle n \rangle$ under constraint in (a), showing resemblance for SSNS and KS. (d) The variance remains independent of θ and overlaps along points in (a), for SSNS ($n = 1$) with $\psi_{KS}^1(+)$. For illustration, we use two sets of points with parameters r and β : $(r, \beta) = (0.15, 1.0)$ represented by the thick line and $(0.6, 2.07)$ denoted by the dotted line.

by probes which provide the same precision in estimating parameters. A probe yielding the same precision of parameter with a smaller energy cost is a better quantum resource in metrology than other probes with larger costs.

For comparison, we show regions for both SSDNS and SSNS where the variance for each state equals that for their respective KS. Figures 4(a)–4(d) describe the resemblance of different quantities: variance, average photon number, and θ dependence of variance for SSDNS and $\psi_{KS}^0(-)$. F_Q is dependent on the θ orientation of displacement in phase space for SSDNS with $n = 1$ and $\psi_{KS}^0(-)$. We obtain two constraints by comparing θ dependent and independent terms for $F_Q(\psi_1)$ and $F_Q(\psi_{KS}^0(-))$. Figure 4(a) plots these between α and β , while squeezing r is dependent on both α and β . Here, β is the absolute of coherent amplitude $\beta e^{i\pi/4}$. This region provides the value of r and α in terms of β , which allows us to plot $\langle n \rangle$ against β in Fig. 4(b). The same variance region shows the same $\langle n \rangle$ for both states. In Fig. 4(c), overlapping lines for the product of variance and $\langle n \rangle$ for both states at respective θ demonstrate resemblance, which is also clear from Figs. 4(a) and 4(b). Irrespective of θ , all lines asymptotically approaching 0.5 describe the asymptotic inverse relation of variance with $\langle n \rangle$ for large β , consistent with the region in Fig. 4(a). This asymptotic behavior for variance and average number is

known as HL sensitivity for KS, resembling SSDNS in the region of equal variance in Fig. 4(a). The variance changes with θ for $\psi_{\text{KS}}^0(-)$ with small $\beta = 1.01$ and becomes almost constant for same state with $\beta = 2.02$. This behavior is exactly mimicked by SSDNS (ψ_1) with $n = 1$, as seen in Fig. 4(d), where r and α are obtained from constraints in Fig. 4(a).

Similarly, the comparison between SSNS and $\psi_{\text{KS}}^l(+)$ can be seen in Figs. 5(a)–5(d). Figures 5(a)–5(d) include a comparison between SSNS and KS for two pairs: SSNS ($n = 1$) and ψ_{KS}^1 , and SSNS ($n = 2$) and ψ_{KS}^2 . In this case, F_Q remains independent of θ for SSNS as well as $\psi_{\text{KS}}^l(+)$ with any n and l . Later in this section, we see that F_Q has θ dependence due to nonzero coefficients in the probes' Fock basis expansion. We obtain two curves corresponding to equal variance for SSNS and KS in each pair: ($n = 1, l = 1$) blue line and ($n = 2, l = 2$) red line in Fig. 5(a). In Fig. 5(b), the average number ($\langle n \rangle$) has overlapping curves for states SSNS $n = 1$ (yellow) and KS $l = 1$ (black), as well as for the other pair SSNS $n = 2$ (blue) and KS $l = 2$ (red), showing identical behavior under the constraint in Fig. 5(a). Similarly, the variance multiplied by the average number demonstrates resemblance in behavior [Fig. 5(c)] for both pairs: $n = 1, l = 1$ (yellow, black) and $n = 2, l = 2$ (blue, red). Asymptotically, all curves approaching 0.5 show HL sensitivity of KS as well as SSNS. Finally, Fig. 5(d) illustrates θ -independent variance for both states $n = 1$ and $l = 1$ at two different points, satisfying the constraint in Fig. 5(a).

We observe that the variance or F_Q displays a dependence on θ , which arises from the decomposition of ψ with zero coefficients in the Fock basis. This dependence can be derived from the second-order derivative of $O_{\nu\delta}$ for $|\psi\rangle = \sum_{n=0}^{\infty} c_n |n\rangle$, with the constraint that the coefficients c_n satisfy $c_n c_m \neq 0$ for $|n - m| \leq 2$. This condition holds true for SSDNS and $\psi_{\text{KS}}^l(-)$, whereas for SSNS and $\psi_{\text{KS}}^l(+)$, the coefficients follow $c_n c_m = 0$ for $|n - m| \leq 2$, resulting in their θ independence.

In this section, we have shown that the fidelities for SSDNS and SSNS, when analyzed with KS, exceed 99%. All these plots in Figs. 4 and 5 describe small phase-space fluctuation measurements corresponding to the same HL sensitivity with the obtained parameters' region of equal variance for both proposed states when compared to the KS.

V. USE OF PROBE IN THE DAMPING CONSTANT ESTIMATION

In the open system, light interacting with the environment such as absorption media, passing through a beam splitter (BS), causes its damping and leads to the decoherence of the quantum state. In this process of coherence loss, it allows us to gain the information about the damping parameter of the medium. The decay of the light amplitude in the cavity is described by the master equation,

$$\frac{\partial \rho}{\partial t} = \kappa(2a\rho a^\dagger - \{a^\dagger a, \rho\}),$$

where κ is the damping constant of the cavity. This equation also describes the dynamics of the BS, opening the possibility to estimate either reflectivity ($1 - \eta$) or transmittivity ($\eta = e^{-2\kappa t}$) of the BS. The use of the quantum state of light

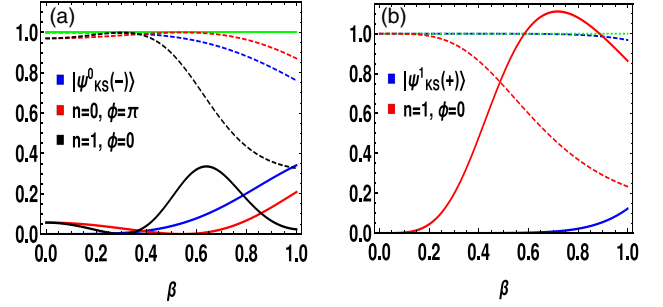


FIG. 6. The regions of the pairs (a) SSDNS and $\psi_{\text{KS}}^0(-)$ and (b) SSNS and $\psi_{\text{KS}}^1(+)$ show values of $\Delta^2 N / \langle N \rangle^2$ (thick) and $\langle N \rangle^{-1}$ (dashed), which closely resemble single-photon states. (a) β for both SSDNS: $S[r](D[\alpha] + D[-\alpha])|1\rangle$ (black) and $S[r](D[\alpha] - D[-\alpha])|0\rangle$ (red) with squeezing $r = 0.1$ represents α , while coherent amplitude for $\psi_{\text{KS}}^0(-)$ (blue). (b) β for SSNS (red) with $n = 1$ is squeezing (r), and coherent amplitude $\psi_{\text{KS}}^1(+)$ (blue). Both (a) and (b) have regions for parameter β , where $\Delta^2 N / \langle N \rangle^2 \rightarrow 0$ and $\langle N \rangle^{-1} \rightarrow 1$.

being sensitive to the small changes in the parameter (κ) can increase the precision of estimating parameter κ . Error ($\Delta\kappa$) associated in the measurement of η , obtained through the output of the BS [28], can be found using the error-propagation method,

$$\Delta\kappa = \frac{\sqrt{\Delta^2 \hat{N}_{\text{out}}}}{|\partial \langle \hat{N}_{\text{out}} \rangle / \partial \kappa|} = \sqrt{\frac{\Delta^2 \hat{N}_{\text{in}}}{4t^2 \langle \hat{N}_{\text{in}} \rangle^2} + \frac{(\eta^{-1} - 1)}{4t^2 \langle \hat{N}_{\text{in}} \rangle}},$$

where $\langle \hat{N}_{\text{out}} \rangle$ ($\langle \hat{N}_{\text{in}} \rangle$) and $\Delta^2 \hat{N}_{\text{out}}$ ($\Delta^2 \hat{N}_{\text{in}}$) are the average number and number variance, respectively, at the output (input) for the probe passing through the BS for time t . As is known, for the optical probe state, Fock states $|n\rangle$ provide the lowest error bound as the number variance is zero with the cost of n average photon number. Hence, the use of a single-photon state leads to the lowest bound with the least cost of 1 ($\langle a^\dagger a \rangle$). We know from Fig. 1 that with an increase in the superposition number of different coherent states (for example, $\sum_{k=0}^{\max} |\alpha_k\rangle$), there is a corresponding larger gap for adjacent nonzero probability in the Fock space. It leads to a decrease in number fluctuation and therefore close to the number state $|n\rangle$. $\Delta\kappa$ depending on the variance and average reaches the minimum for small magnitude β with states SSDNS and $\psi_{\text{KS}}^0(-)$, as well as SSNS $\psi_{\text{KS}}^1(+)$, similar to the single-photon state, which is clearly evident in Fig. 6. As a result, these states as the probes are good candidates to estimate the damping constant of the BS.

VI. PREPARATION OF THE STATE

We now focus on the generation of the proposed states in the optical setup. One procedure, described in detail [29] for the preparation of any single-mode radiation field's state, can be used in our case of both proposed states. This method requires N two-level atoms and high- Q cavity such that the damping of photons and the spontaneous emission rate of atoms in the cavity are negligible. The cavity is initialized in a vacuum state while allowing atoms prepared in superposition states of two levels beforehand to pass through the cavity one by one. Atoms interact via the Jaynes-Cummings-

Hamiltonian with the cavity field state, increasing the Fock state superposition by one, when found in the ground state as they leave the cavity. Tuning parameter d in the two-level atom prepared state $|e\rangle + d|g\rangle$ allows effective control of the amplitude of the Fock state superposition formed in the cavity and hence leads to the desired state preparation after N atoms enter and leave the cavity one by one. To obtain maximum overlap of the formed state in the cavity with the desired state, N must be greater than the average of the photon number for the desired state. It can also be decided from the probability number distribution as the trend becomes appreciably small after obtaining the desired state.

Light-matter interactions have allowed the generation of nonclassical states of light within rotating-wave approximation and beyond RWA. An extensive amount of theoretical research has been performed in solving the dynamics of the JC-Rabi model, but the realization of this model in and beyond ultrastrong coupling (USC) has shown itself to be quite challenging to reach in cavity QED. Advances in technology have allowed uses of a superconducting qubit in circuit QED to simulate dynamics of the Rabi model in the USC regime, as proposed in Ref. [30] and recently reported in Refs. [31–34]. The Hamiltonian for the superconducting qubit-resonator interaction describing the Rabi model in circuit QED in the presence of two-photon driving is

$$\mathcal{H}_1 = \omega_o a^\dagger a + \frac{\omega_a}{2} \sigma_z + g(a^\dagger + a)\sigma_x + G(a^{+2} e^{-2i\omega_t t} + a^2 e^{2i\omega_t t}),$$

where ω_o , ω_a , and ω_t are resonator mode, qubit frequency, and two-photon drive frequency. The annihilation (a or a^-) and creation (a^+) operators belong to the field, while the Pauli matrices (σ_i for $i \in \{1, 2, 3\}$) correspond to the qubit. The parameters g and G describe the interaction strength and two-photon drive strength. This Hamiltonian \mathcal{H} can be further modified by using squeeze $S[\chi] = \exp(\frac{-\chi a^{+2} + \chi^* a^2}{2})$ and displacement $D[\lambda] = \exp(\lambda a^\dagger - \lambda a)$ unitary operators [35] and their respective adjoints $S^+[\chi]$ and $D^+[\lambda]$. For the Hamiltonian involving qubit σ_i for $i \in \{1, 2, 3\}$ and field mode (a^\pm) as separate parties, we have $[\sigma_i, a^\pm] = 0$. We use operators $D[\lambda\sigma_i] = e^{(\lambda\sigma_i a^\dagger - \lambda^* \sigma_i a)} = e^{\sigma_i(\lambda a^\dagger - \lambda^* a)}$ and $S[\chi\sigma_i] = e^{(\frac{\chi}{2}\sigma_i a^2 - \frac{\chi^*}{2}\sigma_i a^{+2})} = e^{\sigma_i(\chi^* a^2 - \chi a^{+2})/2}$ to simplify the Hamiltonian. The diagonalized Hamiltonian reads as

$$\begin{aligned} \mathcal{H}_d &= e^{i\omega_t t a^\dagger a} D^+[\lambda\sigma_x] e^{-i\omega_t t a^\dagger a} S^+[\chi] e^{i\omega_t t a^\dagger a} (\mathcal{H}_1 \\ &\quad - \omega_a \sigma_z / 2) e^{-i\omega_t t a^\dagger a} S[\chi] e^{i\omega_t t a^\dagger a} D[\lambda\sigma_x] e^{-i\omega_t t a^\dagger a} \\ &= \sqrt{\Lambda^2 - 4G^2} a^\dagger a + \frac{1}{2} (\sqrt{\Lambda^2 - 4G^2} - 1) \\ &\quad - \frac{2g^2}{\sqrt{\Lambda^2 - 4G^2}} \left(\frac{\Lambda - 2G}{\Lambda + 2G} \right)^2, \end{aligned}$$

where the parameters detuning (Λ), phase-space displacement (λ), and squeezing coefficient (χ) for the diagonalization of \mathcal{H}_1 (when $\omega_a = 0$) are defined as follows:

$$\begin{aligned} \Lambda &= \omega_o - \omega_t, \quad \lambda = \frac{g(\Lambda - 2G)}{(\sqrt{\Lambda^2 - 4G^2})(\Lambda + 2G)}, \\ \chi &= -\frac{1}{2} \ln \left(\frac{\Lambda + 2G}{\Lambda - 2G} \right). \end{aligned}$$

In the presence of a degenerate qubit (i.e., $\omega_a = 0$), the above Hamiltonian (\mathcal{H}) can be diagonalized in the squeezed displaced number state $S(\chi)[D(\lambda) \pm D(-\lambda)]|n, \pm\rangle$ in the even (odd) parity branches, as discussed in [36]. The introduction of a qubit with $\omega_a \neq 0$ lifts the degeneracy and its eigenspectrum can be approached through first-order perturbation [37], considering the qubit σ_z term as perturbation. This regime is described as perturbative-deep strong coupling. In this regime, for $\omega_a \leq \sqrt{\Lambda^2 - 4G^2}$ [36,37], the above-found eigenstates have a 99% overlap with exact numerically simulated states in Ref. [36] with lifted degeneracy. The generation and properties of the first proposed state have also been theoretically discussed on the ion trap platform [38].

The production of SSNS can be achieved with the help of a system containing two excitations, emissions, and losses of the resonator (oscillator) mode. The two-photon Rabi model has received theoretical interest and was proposed in circuit QED, for example, zero current bias in the superconducting quantum interference device (SQUID) loop controls the linear interacting term, leading to a two-photon-qubit dominant term for the SQUID-flux qubit [39] interaction. The use of the Hamiltonian in the form

$$\mathcal{H}_2 = [g_1 a^\dagger a + g_2 (a^2 + a^{+2})] \sigma_z + \omega a^\dagger a,$$

containing the interaction term of the two-quanta resonator mode with superconducting qubit, can be diagonalized in the interaction picture. The time evolution of the state ($|\psi_I\rangle = e^{ig_1 t \sigma_z a^\dagger a} |\psi_{\mathcal{H}_2}\rangle = U |\psi_{\mathcal{H}_2}\rangle$) is given by

$$\begin{aligned} |\psi_I(t)\rangle &= e^{-i \int_0^t dt U [g_2 (a^2 + a^{+2}) \sigma_z + \omega a^\dagger a] U^{-1}} |\psi_I(0)\rangle \\ &= e^{ig_1 \sigma_z t a^\dagger a / 2} S(-r \sigma_z) e^{-i \frac{t}{2} [(2a^\dagger + a) \sqrt{\omega^2 - 4g_2^2 j_0^2(g_1 t)}]} \\ &\quad \times e^{i \frac{\omega t}{2}} S(r \sigma_z) e^{-ig_1 \sigma_z t a^\dagger a / 2} |\psi_I(0)\rangle, \end{aligned}$$

where the zeroth spherical Bessel function $j_0(t) = t^{-1} \sin t$ and the squeezing parameter $r = \frac{1}{2} \ln \left(\frac{\omega - 2g_2 j_0(g_1 t)}{\omega + 2g_2 j_0(g_1 t)} \right)$, with g_2 being constrained by the condition $2g_2 \leq \omega$ for real r . Initializing the resonator mode and qubit state as $|\psi_I(0)\rangle = |n, +\rangle$, the system's state under \mathcal{H}_2 evolves to the state at time t :

$$\begin{aligned} |\psi_{\mathcal{H}_2}(t)\rangle &= \mathcal{N} S(-re^{-ig_1 \sigma_z t} \sigma_z) S(re^{-i\hat{A}t} \sigma_z) e^{-ig_1 \sigma_z t a^\dagger a} |n, +\rangle \\ &= \mathcal{N} [S(-re^{-ig_1 t}) S(re^{-i\lambda t}) e^{-ig_1 t n} |n, e\rangle \\ &\quad + S(re^{ig_1 t}) S(-re^{-i\lambda t}) e^{ig_1 t n} |n, g\rangle], \end{aligned}$$

where \mathcal{N} corresponds to the normalization constant of the state, and $\hat{A} = g_1 \sigma_z + 2\sqrt{\omega^2 - 4g_2^2 j_0^2(g_1 t)}$ with eigenvalues $\lambda_\pm = \pm g_1 + 2\sqrt{\omega^2 - 4g_2^2 j_0^2(g_1 t)}$ satisfies $\hat{A}|e\rangle$ ($\hat{A}|g\rangle$) = $\lambda_+|e\rangle$ ($\lambda_-|g\rangle$). Measurement of the qubit of the above evolved state in a $|\pm\rangle$ basis will lead to the required superposition of the squeezed number state.

VII. CONCLUSION

We compared the number distribution (PND), Wigner function, fidelity, and sensitivity of SSNS and SSDNS with the compass state (KS). The investigation of these properties has led to the finding that appropriate squeezing r and displacement α show close number distribution, similar Wigner

function, and maximum fidelity with the KS, $\psi_{\text{KS}}^l(\pm)$. The PND shows zero and nonzero probability amplitudes with respect to the values of l , just as SSNS and SSDNS exhibit comparable behavior depending on the values of r , α , and the Fock number n . Similarly, the Wigner distribution corresponding to the SSNS and SSDNS produces Gaussian lobes with interferometric structure, closely identical to the KS. Both the PND and the Wigner function behavior of the SSDNS and SSNS allow us to have KSs with different weight factors denoted by l , leading to a large overlap. We find a change in the behavior of the phase-space distribution for SSDNS (ψ_1) and KS as well as a decrease in the fidelity with KS below 99%, as seen in Table I, when the Fock number $n \neq 1$. Our other state SSNS (ψ_2), with the squeezing r and the Fock number n , shows resemblance in its interferometric phase-space distribution close to that of the KS. Increasing the parameter n of SSNS leads to fidelity above 99% and an increase in the β amplitude of the KS. We see that SSDNS with $n = 1$ and SSNS with $n > 0$ provide a large overlap with KS, showing potential for reaching close to the KS with a coherent amplitude $\beta > 0.5$. Furthermore, the use of KS in detecting small perturbation is no better than SSDNS and SSNS as there exist regions, in the parameter space of squeezing, displacement, and coherent amplitude of equal variances with equal average energy, evident from Figs. 4 and 5.

It is noteworthy to mention that the single-photon state has recently shown to be the best probe in the small shift parameter estimation [26] as well as in estimating the damping constant [28] for the amplitude damping channel. In view of the difficulties with the generation of the single-photon state, SSNS, SSDNS, and KS provide the same precision, in the limit of small β , for the estimation of the damping parameter of the BS (see Fig. 6), close to the single-photon state, thereby becoming probes next to the single-photon state. Due to their same sensitivity to small shifts, states used as qubits in quantum error correction can recognize errors originating as minute phase-space displacements caused by noise external to the system. The ability to correct these errors is a work in progress and will be demonstrated elsewhere.

Given the challenges present in obtaining large coherent amplitudes (β) of the KS, there are few models to produce KS states directly either in an optical platform such as Kerr interaction and conditional measurement on the BS [24,40] or in the microwave regime. Therefore, considering their many implications, theoretical models are provided based on their accessibility in the optical as well as circuit QED. Sub-Planck structures in SSDNS and SSNS, and their co-relation to the compass state, will enable different methods for the preparation of such states, which may find applications in quantum metrology, sensing, communication, and error correction.

ACKNOWLEDGMENT

A. is thankful to the University Grants Commission and Council of Scientific and Industrial Research, New Delhi, Government of India for the Junior Research Fellowship at IISER Kolkata.

TABLE II. Comparison of the fidelities of SSDNS and SSNS with KS for parameters used in Sec. III of Wigner functions.

State $\mathcal{F}_{\psi}^{(l,\pm)}$	α	n	r	KS (β)	Fidelity ($\mathcal{F}_{\psi}^{(l,\pm)}$)
$\mathcal{F}_{\psi_2}^{(0,+)}$	0	4	0.45	2	0.7206
$\mathcal{F}_{\psi_2}^{(3,+)}$	0	3	0.45	2	0.97
$\mathcal{F}_{\psi_2}^{(2,+)}$	0	2	0.45	1.5	0.9816
$\mathcal{F}_{\psi_2}^{(1,+)}$	0	1	0.45	1.5	0.9812
$\mathcal{F}_{\psi_1}^{(0,-)}$	2	4	0.45	$2e^{3i\pi/4}$	0.104
$\mathcal{F}_{\psi_1}^{(0,-)}$	2	3	0.45	$2e^{3i\pi/4}$	0.1363
$\mathcal{F}_{\psi_1}^{(1,-)}$	2	2	0.45	$1.7e^{3i\pi/4}$	0.3147
$\mathcal{F}_{\psi_1}^{(1,-)}$	2	1	0.45	$1.7e^{3i\pi/4}$	0.9865

APPENDIX A: FIDELITIES FOR THE WIGNER FUNCTION IN SEC. III

It is evident from Fig. 2 that the Wigner function of the first states, along with their comparison with the KS, illustrates a resemblance in the phase-space structure. Additionally, their fidelity, as presented in Table II, starts decreasing with increasing Fock number n .

Regarding the SSNS, the Wigner functions in Fig. 3, along with their comparison with the KSs, exhibit significant resemblance and a large overlap (Table II) with each other. Although the fidelity of SSNS (ψ_2) with $n = 4$ is reduced to 0.7206 for $\beta = 2$ (the amplitude of KS), this can be optimized to achieve a large overlap for $\beta > 2$, as the phase-space area of states increases with larger n .

APPENDIX B: CALCULATIONS FOR THE QUANTITIES IN THE MAIN TEXT

We find the x projection of the squeezed and displaced state ($\psi(x) = \langle x|S[r]D[\alpha]|0\rangle$) by solving the differential equation of the annihilation operator \hat{a} as follows:

$$S[r]D[\alpha]\hat{a}D[-\alpha]S[-r]S[r]D[\alpha]|0\rangle = 0.$$

For real squeezing (r) and complex displacement (α), the above equation in x space using the displacement identity $D(i\text{Im}[\alpha])D(\text{Re}[\alpha]) = D[\alpha]e^{i\text{Re}[\alpha]\text{Im}[\alpha]}$ turns into

$$(\partial_x e^{-r} + x e^r - \sqrt{2}\alpha)\psi(x) = 0,$$

leading to

$$\psi(x) = \frac{1}{\sqrt[4]{(\pi e^{-2r})}} e^{-\frac{(x e^r - \sqrt{2}\alpha)^2}{2} - \text{Im}[\alpha]^2} e^{-i\text{Re}[\alpha]\text{Im}[\alpha]}.$$

The zeroth-state weight factor in the squeezed displaced state $\psi(x)$ is given by

$$c_0(r, \alpha) = \langle 0|S[r]D[\alpha]|0\rangle = \frac{e^{-\frac{\alpha^2}{e^{2r}+1} + i\alpha\text{Im}[\alpha]}}{\sqrt{\cosh(r)}}.$$

We know from the main text that SSDNS with a real displacement parameter is written as α ,

$$\psi_1(x) = \langle x|\psi_1\rangle = N_1[\phi_n(e^r x - \alpha) + \phi_n(e^r x + \alpha)],$$

TABLE III. Symbols used in the main text.

$I_{nm}(r_1, r_2, \alpha, \beta) = \frac{Nr_{n,m,k}^{\phi,r_1,r_2}(\alpha,\beta,0)}{\sqrt{Nr_{n,n,k}^{\phi,r_1,r_1}(\alpha,\alpha,0)Nr_{m,m,k}^{\phi,r_2,r_2}(\beta,\beta,0)}} \Bigg _{\substack{k=0 \\ \phi=0}}$	$\bar{I}_n(r, \alpha, \beta) = \frac{Nr_{n,n,k}^{\phi,r,r}(\alpha,\beta,0)}{\sqrt{Nr_{n,n,k}^{\phi,r,r}(\alpha,\alpha,0)Nr_{n,n,k}^{\phi,r,r}(\beta,\beta,0)}} \Bigg _{\substack{k=0 \\ \phi=0}}$
$w_{nm}(r_1, r_2, \alpha, \beta) = \frac{C_{n,m,k}^{\phi,r_1,r_2}(\alpha,\beta,0,z)}{\sqrt{Nr_{n,n,k}^{\phi,r_1,r_1}(\alpha,\alpha,0)Nr_{m,m,k}^{\phi,r_2,r_2}(\beta,\beta,0)}} \Bigg _{\substack{k=0 \\ \phi=0}}$	$w_n(r, \alpha, \beta) = \frac{C_{n,n,k}^{\phi,r,r}(\alpha,\beta,0,z)}{\sqrt{Nr_{n,n,k}^{\phi,r,r}(\alpha,\alpha,0)Nr_{n,n,k}^{\phi,r,r}(\beta,\beta,0)}} \Bigg _{\substack{k=0 \\ \phi=0}}$
$\text{Tr}[D[\delta]\hat{O}] = \frac{Nr_{n,n,k}^{\phi,r_1,r_2}(\alpha,\beta,\delta)}{\sqrt{Nr_{n,n,k}^{\phi,r_1,r_1}(\alpha,\alpha,0)Nr_{m,m,k}^{\phi,r_2,r_2}(\beta,\beta,0)}} \Bigg _{\substack{k=0 \\ \phi=0}}$	$\text{Tr}[(a^\dagger a)^k \hat{O}] = \frac{Nr_{n,n,k}^{\phi,r_1,r_2}(\alpha,\beta,0)}{\sqrt{Nr_{n,n,k}^{\phi,r_1,r_1}(\alpha,\alpha,0)Nr_{m,m,k}^{\phi,r_2,r_2}(\beta,\beta,0)}} \Bigg _{\phi=0}$

while SSNS, depending on the squeezing parameters ($\pm r$), is

$$\psi_2(x) = \langle x|\psi_2\rangle = N_2[\phi_n(e^r x) + \phi_n(e^{-r} x)].$$

The normalization N_1 and N_2 for both states is given as

$$N_1^{-2} = \bar{I}_n(r, \alpha, -\alpha) + \bar{I}_n(r, -\alpha, \alpha) + \bar{I}_n(r, -\alpha, -\alpha) + \bar{I}_n(r, \alpha, \alpha)$$

and

$$N_2^{-2} = I_{nn}(r, -r, 0, 0) + I_{nn}(r, -r, 0, 0) + \bar{I}_n(r, 0, 0) + \bar{I}_n(-r, 0, 0),$$

with symbols, for $r \neq \bar{r}$,

$$I_{nm}(r, \bar{r}, \alpha, \beta) = \int_{-\infty}^{\infty} dx \phi_n(e^r x - \sqrt{2}\alpha)\phi_m^*(e^{\bar{r}} x - \sqrt{2}\beta),$$

and for $r = \bar{r}$,

$$\bar{I}_n(r, \alpha, \beta) = \int_{-\infty}^{\infty} dx \phi_n(e^r x - \sqrt{2}\alpha)\phi_n^*(e^r x - \sqrt{2}\beta).$$

The above integrals are evaluated using the identity obtained through the generating function (see Table III) of the Hermite polynomials [41].

Calculations for the number distribution based on the above quantities are

$$c_k = \langle k|\psi_1\rangle = N_1[I_{nk}(r, 0, \alpha, 0) + I_{nk}(r, 0, -\alpha, 0)]$$

and

$$b_k = \langle k|\psi_2\rangle = N_2[I_{nk}(r, 0, 0, 0) + I_{nk}(-r, 0, 0, 0)].$$

The Wigner function calculations are

$$W_1(x, p) = \frac{1}{\pi} \int_{-\infty}^{\infty} dy \langle x-y|\psi_1\rangle \langle \psi_1|x+y\rangle e^{2ipy} = N_1^2[w_n(r, \alpha, \alpha) + w_n(r, -\alpha, -\alpha) + w_n(r, \alpha, -\alpha) + w_n(r, -\alpha, \alpha)]$$

and

$$W_2(x, p) = \frac{1}{\pi} \int_{-\infty}^{\infty} dy \langle x-y|\psi_2\rangle \langle \psi_2|x+y\rangle e^{2ipy} = N_2^2[w_n(r, 0, 0) + w_n(-r, 0, 0) + w_{nn}(r, -r, 0, 0) + w_{nn}(-r, r, 0, 0)],$$

where $W_1(x, p)$ and $W_2(x, p)$ are the Wigner functions for states $|\psi_1\rangle$ and $|\psi_2\rangle$, respectively. The functions used above,

$$w_{nm}(r, \bar{r}, \alpha, \beta) = \frac{1}{\pi} \int_{-\infty}^{\infty} dy \phi_n[e^r(x-y) - \sqrt{2}\alpha] \times \phi_m^*[e^{\bar{r}}(x+y) - \sqrt{2}\beta] e^{2ipy}$$

and

$$w_n(r, \alpha, \beta) = \frac{1}{\pi} \int_{-\infty}^{\infty} dy \phi_n[e^r(x-y) - \sqrt{2}\alpha] \times \phi_n^*[e^r(x+y) - \sqrt{2}\beta] e^{2ipy},$$

are evaluated in Table III. Similarly, the Wigner function (W_{KS}) for the compass state $|\psi_{KS}(\pm)\rangle$ includes 16 terms of Gaussian integrals [1]. Number distribution and Wigner function are obtained through the evaluation of the cross term as follows:

$$C_{n,m,k}^{\phi,r_1,r_2}(\alpha, \beta, \delta, z) = \int_{-\infty}^{\infty} d^2\gamma \frac{\langle -\gamma|e^{i\phi a^\dagger a} D[\delta]\hat{O}|\gamma\rangle}{e^{-2(\gamma^*z - z^*\gamma) - 2|z|^2}} = \frac{\partial_\phi^k \partial_s^n \partial_t^m}{(ik\sqrt{n!m!})} \left\{ \int_{-\infty}^{\infty} d^2\gamma e^{i\text{Im}[e^{-i\phi}\gamma\delta^* - |\alpha|^2 + (\bar{\alpha}-s)(s+\alpha^*)]} \times c_0(r_1, \bar{\alpha})c_0^*(r_2, \bar{\beta}) \frac{e^{-e^2\gamma^*\beta + (\bar{\beta}^* - t)t}}{e^{-2(\gamma^*z - z^*\gamma) - 2|z|^2}} e^{\frac{s^2+t^2}{2}} \right\} \Bigg|_{\substack{s=0 \\ t=0}}$$

where $z = x + ip$, $\hat{O} = S[r_1]D[\alpha]|n\rangle\langle m|D[-\beta]S[-r_2] = (\partial_s^n \partial_t^m S[r_1]D[\alpha]|s\rangle\langle t|D[-\beta]S[-r_2] \frac{e^{\frac{s^2+t^2}{2}}}{\sqrt{n!m!}})|_{s=0, t=0}$

and

$$\bar{\alpha} = e^{r_1}(\delta + e^{-i\phi}\gamma) + \alpha + s, \bar{\beta} = -e^{r_2}\gamma + \beta + t.$$

The above expression is normalized from the cross term [$C_{n,m,k}^{\phi,r_1,r_2}(\alpha, \beta, \delta, z)$] as

$$Nr_{n,m,k}^{\phi,r_1,r_2}(\alpha, \beta, \delta) = \int_{-\infty}^{\infty} d^2z C_{n,m,k}^{\phi,r_1,r_2}(\alpha, \beta, \delta, z).$$

Using these quantities above, we write the symbols I_{nm} and w_{nm} in Table III.

The two expressions in the last row, which are the cross terms, are used to evaluate the overlap ($\mathcal{F}_{\psi}^{(l,\pm)}, Ov_{\delta}$) between the perturbed and unperturbed states, average photon number, and number variance.

-
- [1] W. Zurek, Sub-Planck structure in phase space and its relevance for quantum decoherence, *Nature (London)* **412**, 712 (2001).
- [2] The kitten state, akin to the cat and compass states, exhibits low coherent amplitudes ($\beta < 0.5$, corresponding to half of the quadrature variance for coherent states), resulting in an identical phase distribution resembling four Gaussian lobes. Both the cat and compass states, characterized by the same parity and low amplitude, demonstrate underdeveloped interference, resulting in four Gaussian lobes that mimic the compass state within the cat state. To address potential label ambiguity in coherent, cat, and compass states, we introduce the “KS” label derived from the kitten state for both compass and kitten states. While our primary focus in this paper remains to achieve large-amplitude compass states, instances of lower β values for the output compass state labeled as KS indicate the kitten state. Notably, these cases are identified through the Fisher information F_Q , as illustrated later in Figs. 4(a) and 5(a) in Sec. IV.
- [3] D. Dalvit, R. de Matos Filho, and F. Toscano, Quantum metrology at the Heisenberg limit with ion trap motional compass states, *New J. Phys.* **8**, 276 (2006).
- [4] J. R. Bhatt, P. K. Panigrahi, and M. Vyas, Entanglement-induced sub-Planck phase-space structures, *Phys. Rev. A* **78**, 034101 (2008).
- [5] P. K. Panigrahi, A. Kumar, U. Roy, and S. Ghosh, Sub-Planck structures and quantum metrology, *AIP Conf. Proc.* **1384**, 84 (2011).
- [6] F. Toscano, D. A. R. Dalvit, L. Davidovich, and W. H. Zurek, Sub-Planck phase-space structures and Heisenberg-limited measurements, *Phys. Rev. A* **73**, 023803 (2006).
- [7] L. G. Lutterbach and L. Davidovich, Method for direct measurement of the Wigner function in cavity QED and ion traps, *Phys. Rev. Lett.* **78**, 2547 (1997).
- [8] A. Luis, Heisenberg limit for displacements with semiclassical states, *Phys. Rev. A* **69**, 044101 (2004).
- [9] G. S. Agarwal and K. Tara, Nonclassical properties of states generated by the excitations on a coherent state, *Phys. Rev. A* **43**, 492 (1991).
- [10] Arman, G. Tyagi, and P. K. Panigrahi, Photon added cat state: Phase-space structure and statistics, *Opt. Lett.* **46**, 1177 (2021).
- [11] N. Biagi, S. Francesconi, A. Zavatta, and M. Bellini, Photon-by-photon quantum light state engineering, *Prog. Quantum Electron.* **84**, 100414 (2022).
- [12] S. Puri, S. Boutin, and A. Blais, Engineering the quantum states of light in a Kerr-nonlinear resonator by two-photon driving, *npj Quantum Inf.* **3**, 18 (2017).
- [13] L. A. Howard, T. J. Weinhold, F. Shahandeh, J. Combes, M. R. Vanner, A. G. White, and M. Ringbauer, Quantum hypercube states, *Phys. Rev. Lett.* **123**, 020402 (2019).
- [14] L. Li, C.-L. Zou, V. V. Albert, S. Muralidharan, S. M. Girvin, and L. Jiang, Cat codes with optimal decoherence suppression for a lossy bosonic channel, *Phys. Rev. Lett.* **119**, 030502 (2017).
- [15] W. Cai, Y. Ma, W. Wang, C.-L. Zou, and L. Sun, Bosonic quantum error correction codes in superconducting quantum circuits, *Fundament. Res.* **1**, 50 (2021).
- [16] C. Chamberland, K. Noh, P. Arrangoiz-Arriola, E. T. Campbell, C. T. Hann, J. Iverson, H. Putterman, T. C. Bohdanowicz, S. T. Flammia, A. Keller *et al.*, Building a fault-tolerant quantum computer using concatenated cat codes, *PRX Quantum* **3**, 010329 (2022).
- [17] A. Biswas and G. S. Agarwal, Nonclassicality and decoherence of photon-subtracted squeezed states, *Phys. Rev. A* **75**, 032104 (2007).
- [18] S. Choudhury and P. K. Panigrahi, A proposal to generate entangled compass states with sub-Planck structure, *AIP Conf. Proc.* **1384**, 91 (2011).
- [19] K. Tara, G. S. Agarwal, and S. Chaturvedi, Production of Schrödinger macroscopic quantum-superposition states in a Kerr medium, *Phys. Rev. A* **47**, 5024 (1993).
- [20] J. S. Neergaard-Nielsen, B. M. Nielsen, C. Hettich, K. Mølmer, and E. S. Polzik, Generation of a superposition of odd photon number states for quantum information networks, *Phys. Rev. Lett.* **97**, 083604 (2006).
- [21] G. Kirchmair, B. Vlastakis, Z. Leghtas, S. E. Nigg, H. Paik, E. Ginossar, M. Mirrahimi, L. Frunzio, S. M. Girvin, and R. J. Schoelkopf, Observation of quantum state collapse and revival due to the single-photon Kerr effect, *Nature (London)* **495**, 205 (2013).
- [22] A. Ourjoumtsev, H. Jeong, R. Tualle-Brouiri, and P. Grangier, Generation of optical “Schrödinger cats” from photon number states, *Nature (London)* **448**, 784 (2007).
- [23] E. V. Mikheev, A. S. Pugin, D. A. Kuts, S. A. Podoshvedov, and N. B. An, Efficient production of large-size optical Schrödinger cat states, *Sci. Rep.* **9**, 14301 (2019).
- [24] J. Hastrup, J. S. Neergaard-Nielsen, and U. L. Andersen, Deterministic generation of a four-component optical cat state, *Opt. Lett.* **45**, 640 (2020).
- [25] F. R. Cardoso, D. Z. Rossatto, G. P. L. M. Fernandes, G. Higgins, and C. J. Villas-Boas, Superposition of two-mode squeezed states for quantum information processing and quantum sensing, *Phys. Rev. A* **103**, 062405 (2021).
- [26] W. Górecki, A. Riccardi, and L. Maccone, Quantum metrology of noisy spreading channels, *Phys. Rev. Lett.* **129**, 240503 (2022).
- [27] S. Zhou and L. Jiang, An exact correspondence between the quantum Fisher information and the Bures metric, [arXiv:1910.08473](https://arxiv.org/abs/1910.08473).
- [28] J. Wang, L. Davidovich, and G. S. Agarwal, Quantum sensing of open systems: Estimation of damping constants and temperature, *Phys. Rev. Res.* **2**, 033389 (2020).

- [29] K. Vogel, V. M. Akulin, and W. P. Schleich, Quantum state engineering of the radiation field, *Phys. Rev. Lett.* **71**, 1816 (1993).
- [30] A. Blais, R.-S. Huang, A. Wallraff, S. M. Girvin, and R. J. Schoelkopf, Cavity quantum electrodynamics for superconducting electrical circuits: An architecture for quantum computation, *Phys. Rev. A* **69**, 062320 (2004).
- [31] T. Niemczyk, F. Deppe, H. Huebl, E. Menzel, F. Hocke, M. Schwarz, J.-J. Garcia-Ripoll, D. Zueco, T. Hümmer, E. Solano *et al.*, Circuit quantum electrodynamics in the ultrastrong-coupling regime, *Nat. Phys.* **6**, 772 (2010).
- [32] A. Baust, E. Hoffmann, M. Haeberlein, M. J. Schwarz, P. Eder, J. Goetz, F. Wulschner, E. Xie, L. Zhong, F. Quijandría, D. Zueco, J.-J. Garcia Ripoll, L. García-Álvarez, G. Romero, E. Solano, K. G. Fedorov, E. P. Menzel, F. Deppe, A. Marx, and R. Gross, Ultrastrong coupling in two-resonator circuit QED, *Phys. Rev. B* **93**, 214501 (2016).
- [33] P. Forn-Díaz, J. J. García-Ripoll, B. Peropadre, J.-L. Orgiazzi, M. Yurtalan, R. Belyansky, C. M. Wilson, and A. Lupascu, Ultrastrong coupling of a single artificial atom to an electromagnetic continuum in the nonperturbative regime, *Nat. Phys.* **13**, 39 (2017).
- [34] J. Braumüller, M. Marthaler, A. Schneider, A. Stehli, H. Rotzinger, M. Weides, and A. V. Ustinov, Analog quantum simulation of the rabi model in the ultrastrong coupling regime, *Nat. Commun.* **8**, 1 (2017).
- [35] R. Gutiérrez-Jáuregui and G. S. Agarwal, Probing the spectrum of the Jaynes-Cummings-Rabi model by its isomorphism to an atom inside a parametric amplifier cavity, *Phys. Rev. A* **103**, 023714 (2021).
- [36] D. Z. Rossatto, C. J. Villas-Bôas, M. Sanz, and E. Solano, Spectral classification of coupling regimes in the quantum Rabi model, *Phys. Rev. A* **96**, 013849 (2017).
- [37] J. Casanova, G. Romero, I. Lizuain, J. J. García-Ripoll, and E. Solano, Deep strong coupling regime of the Jaynes-Cummings model, *Phys. Rev. Lett.* **105**, 263603 (2010).
- [38] F. A. El-Orany, Quantum statistical properties of superposition of squeezed and displaced number states, *Czech. J. Phys.* **49**, 1145 (1999).
- [39] S. Felicetti, D. Z. Rossatto, E. Rico, E. Solano, and P. Forn-Díaz, Two-photon quantum Rabi model with superconducting circuits, *Phys. Rev. A* **97**, 013851 (2018).
- [40] G. S. Thekkadath, B. A. Bell, I. A. Walmsley, and A. I. Lvovsky, Engineering Schrödinger cat states with a photonic even-parity detector, *Quantum* **4**, 239 (2020).
- [41] A. Wünsche, Hermite and Laguerre 2D polynomials, *J. Comput. Appl. Math.* **133**, 665 (2001).